Multiangle, multiscale inversion of migrated seismic data

Kees Wapenaar and Jeroen Goudswaard, Delft University of Technology, Delft, The Netherlands
Aart-Jan van Wijngaarden, Norsk Hydro, Bergen, Norway

The relation between the angle-dependent reflectivity of an interface in a target zone and the amplitude-variation-with-offset (AVO) effects observed in the seismic data at the earth's surface is complicated by many factors, as was pointed out in Ostrander's classic paper (Geophysics, 1984). Some factors are "reflection related" (such as thin-bed tuning, reflector curvature), others "propagation related" (such as geometrical spreading, transmission and/or anelastic losses), or "acquisition related" (such as source/receiver directivity, geophone coupling). Amplitude-versus-angle (AVA) inversion in a target zone can be carried out successfully only when these effects are taken into account, either by forward modeling or by stepwise processing prior to AVA inversion. In the Delphi research program, we opt for the latter. For example, by decomposing multicomponent ocean-bottom measurements into *P*- and *S*-wave responses, the effects of receiver directivity are implicitly suppressed. Furthermore, the geometrical spreading effects are compensated for during migration.

The setup of this paper is as follows. We start by reviewing the Delphi approach to AVA inversion for migrated single- and multimode reflection data, assuming that all distorting effects have been optimally eliminated. Then we address the effects of transmission loss and wavelet interference related to fine layering and discuss how to account for these effects in migration. Finally, we introduce a multiscale model for seismic reflectors and indicate how to account for this in inversion.

Multiangle inversion. Migration of multioffset data yields, apart from a structural image, the angle-dependent reflection information for any image point in the subsurface (see article by Berkhout in this issue). Figure 1 shows a structural image, integrated with the angle-dependent reflectivity information along one vertical line of the structural image. To be more precise, the angle-dependent reflectivity information is displayed as a function of depth z and ray parameter p, where p is related to the incidence angle θ and the local propagation velocity c, according to $p = (\sin\theta)/c$. Hence, the data vector **d** (the blue line in Figure 1) represents the reflectivity as a function of p at one particular image point in the subsurface. In the remainder of this section we summarize Van Wijngaarden's 1998 doctoral dissertation at Delft University.

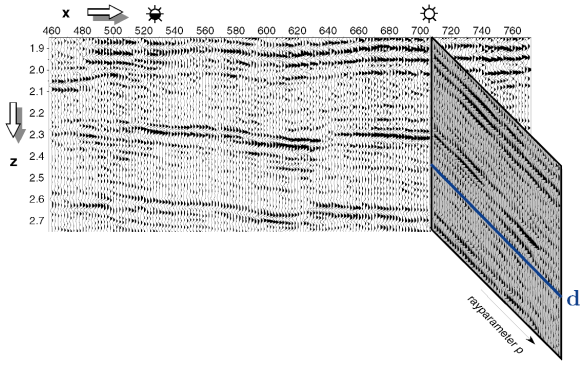

Figure 1. Integration of a structural image and an angle-dependent reflectivity section; d is the data vector used in AVA inversion.

We introduce the *linearized* model $\mathbf{d} = \mathbf{A}\boldsymbol{\lambda} + \mathbf{n}$, where $\mathbf{A}$ is a matrix, derived from the Zoeppritz equation for angle-dependent *PP*-reflectivity, $\boldsymbol{\lambda}$ is a contrast parameter vector, and $\mathbf{n}$ is a "noise vector" that contains all effects that are not accounted for by this linear model. For the contrast parameter vector, we choose $\boldsymbol{\lambda} = (\Delta Z_p/\bar{Z}_p, \Delta c_p/\bar{c}_p, \Delta\mu/\bar{\mu})^T$. Here Z_p, c_p, and μ stand for *P*-wave impedance, *P*-wave velocity, and shear modulus, respectively; Δ denotes the difference of the parameters below and above the interface; and the bar denotes their average value. Note that it may seem more attractive to define the parameter vector in terms of the more basic parameters c_p, c_s (*S*-wave velocity), and ρ (mass density). However, these parameters are not well resolved when only *PP*-data are available. Therefore we reserve the latter parameterization for multimode inversion.

The aim of AVA inversion is to resolve the parameter vector $\boldsymbol{\lambda}$ from the data vector $\mathbf{d}$. To stabilize this process, a priori information can be included in the form of linear relations between the parameters, derived from rock-physics and empirical trends. This a priori information can

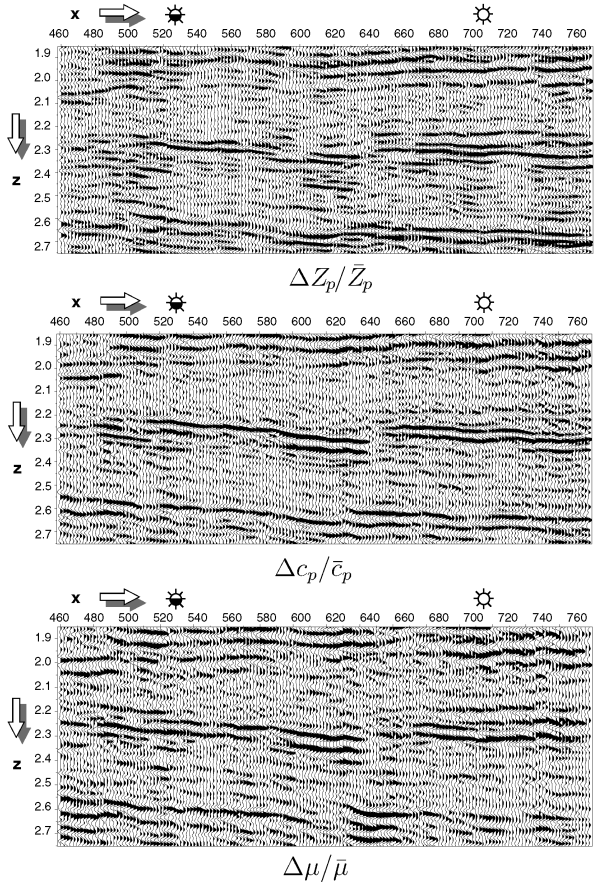

Figure 2. Estimated contrast parameter sections $\Delta Z_p/\bar{Z}_p$, $\Delta c_p/\bar{c}_p$, and $\Delta\mu/\bar{\mu}$.

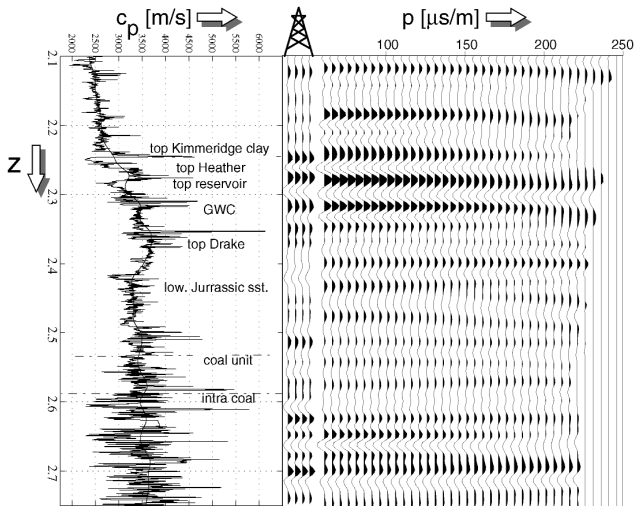

Figure 3. Integration of well-log (P-wave velocity), synthetic impedance contrast, and $\mathbf{A}\boldsymbol{\lambda}_{est}$ for all image points along the well.

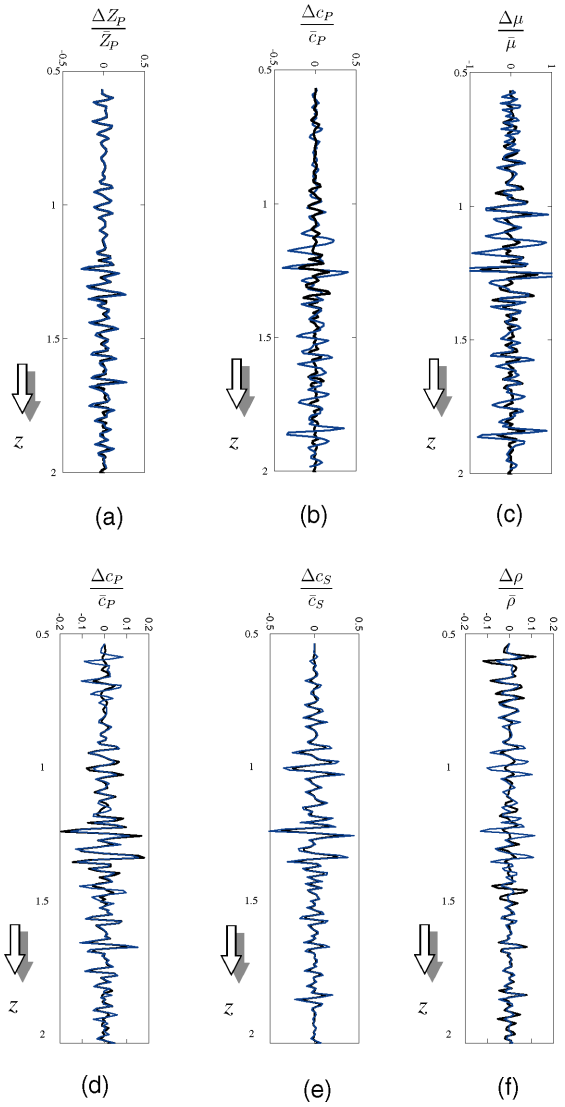

Figure 4. Estimated contrast parameters using single-mode (a-c) and multimode (d-f) inversion. The blue curves are the inversion results, and the black curves have been computed directly from the model.

be formulated as $\mathbf{d}_{ap} = \mathbf{A}_{ap}\boldsymbol{\lambda} + \mathbf{n}_{ap}$. In our least-squares inversion process, vectors $\mathbf{d}$ and $\mathbf{d}_{ap}$ can be given different weights, depending on the confidence that one has in the data and in the a priori information. By repeating the inversion process for all available data vectors $\mathbf{d}$, we obtain the estimated parameter vector $\boldsymbol{\lambda}_{est}$ for all image points of interest. The results can be displayed as depth sections in terms of the contrast parameters $\Delta Z_p/\bar{Z}_p$, $\Delta c_p/\bar{c}_p$, and $\Delta\mu/\bar{\mu}$.

An example is given in Figure 2, which shows these sections, obtained from a 2-D marine data set (offshore mid-Norway). The main target consists of the Jurassic sand-

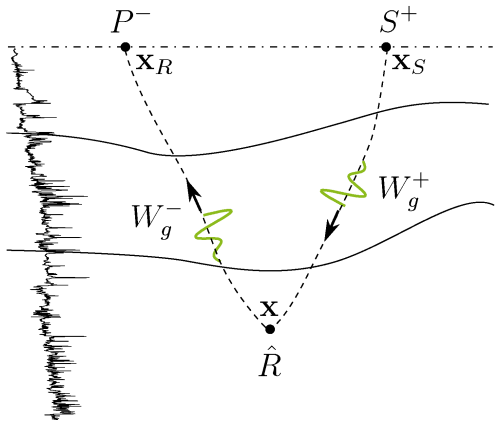

Figure 5. The generalized primary representation for 3-D finely layered media. The dispersion included in the propagators W_g^+ and W_g^- accounts for the "propagation-related" apparent AVA effects in the reflection response P^-.

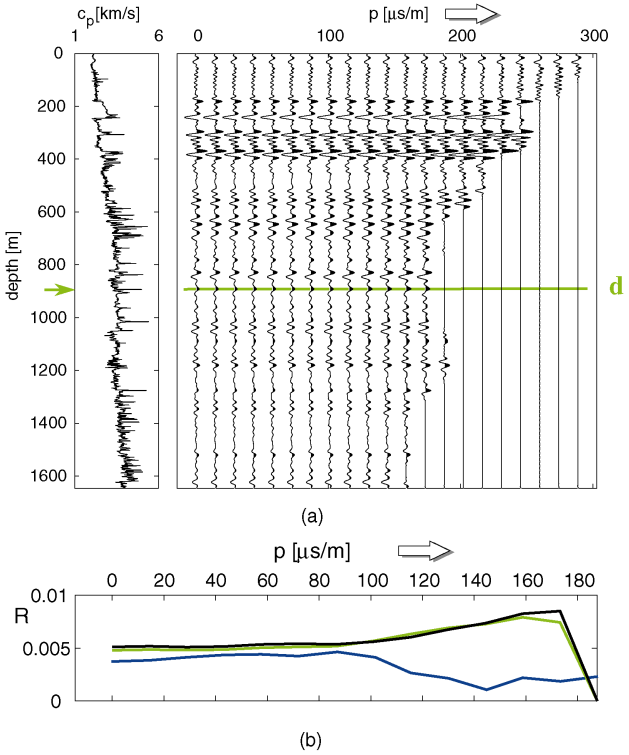

Figure 6. (a) Integration of well-log (P-wave velocity) and angle-dependent reflectivity section, obtained by generalized primary migration. (b) Angle-dependent reflection amplitudes at z = 890 m, obtained by migration without (blue) and with fine-layering corrections (green, obtained from Figure a). The black curve is the exact result.

stones in the two tilted fault blocks. In the *P*-wave velocity contrast section the top (gas) reservoir shows up clearly as a strong reflection around $z = 2.3$ km, with a well defined fault at $x = 650$ m. The impedance contrast section shows a higher resolution, compared to the other two sections, as expected. The three sections together can be used for further lithology discrimination.

To validate the results, we computed $\mathbf{A}\boldsymbol{\lambda}_{est}$ for all image points along one vertical line. This is shown in Figure 3, together with a well log at the same lateral position and a synthetic impedance contrast modeled from the well log, using the adaptive scale-dependent method of Verhelst (1999 doctoral dissertation, Delft University). Overall there is quite a good match, but there are some notable differences as well (e.g., the event just above $z = 2.2$ km in the seismic data does not correspond to an event in the synthetic impedance contrast log). By analyzing the residue section $\mathbf{d} - \mathbf{A}\boldsymbol{\lambda}_{est}$ (not shown), we concluded that the mismatch can be partly attributed to residual multiple reflections (only the surface-related multiples were eliminated prior to migration with a 2-D algorithm).

So far we have considered inversion of *PP* data only. The resolution between the different parameters can be improved when *PS* and/or *SS* data are available as well. In particular the inclusion of migrated *SS* data substantially improves the results. We illustrate this with a numerical example based on well-log data from the North Sea (offshore Norway). We modeled the *PP* and *SS* responses (including internal multiple reflections and mode conversions) of a horizontally layered medium, derived from the blocked well log, and subsequently migrated these data. We adapted the bandwidth of the migrated *SS* data in such a way that both migration results had the same vertical resolution. For each depth this yielded two data vectors, $\mathbf{d}_{PP}$ and $\mathbf{d}_{SS}$. First, the data vectors

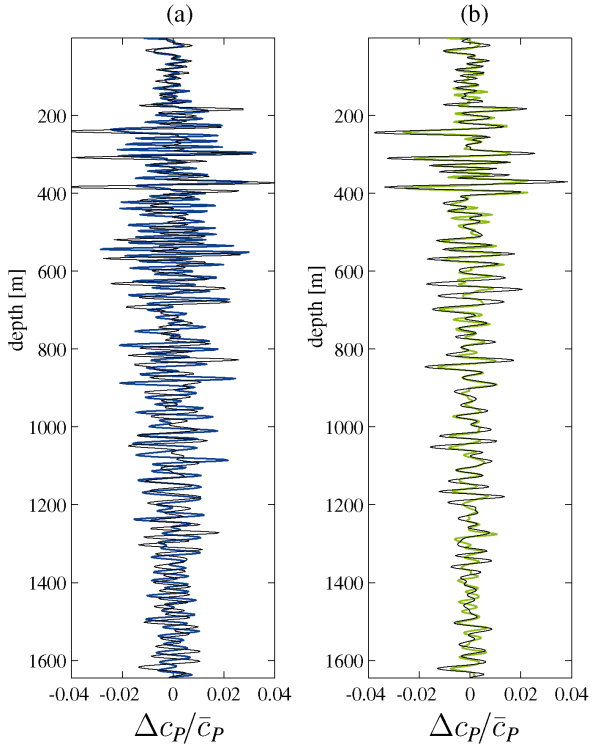

Figure 7. AVA inversion applied to the results of migration without (a) and (b) with fine-layering corrections. The blue and green curves are the inversion results; the black curves are filtered versions of the velocity log.

$\mathbf{d}_{PP}$ were subjected to our inversion algorithm. Figures 4a-c show the estimated contrast parameters (blue) as a function of depth. Note that the match with the exact parameters (black) is very good for $\Delta Z_p/\bar{Z}_p$. The match for the other two parameters is less accurate. Next we inverted $\mathbf{d}_{PP}$ and $\mathbf{d}_{SS}$ simultaneously. Since we expect better resolution, we defined a new parameter vector in terms of the more basic parameters c_p, c_s, and ρ, according to $\boldsymbol{\lambda} = (\Delta c_p/\bar{c}_p, \Delta c_s/\bar{c}_s, \Delta\rho/\bar{\rho})^{\mathrm{T}}$. The results are shown Figures 4d-f. Note that the estimated *P*-wave velocity contrast ($\Delta c_p/\bar{c}_p$) improved significantly in comparison with the single-mode inversion result. Also the match for $\Delta c_s/\bar{c}_s$ is very good. The density contrast is less well resolved.

In summary, seismic migration eliminates the propagation effects from the seismic data. Hence, the data vectors $\mathbf{d}$ contain angle-dependent reflection information at image points in the subsurface rather than offset-dependent information at the surface. Linearized inversion of these data vectors yields the local contrast parameters for any image point in the subsurface. Obviously, the quality of the inversion result depends on the accuracy of the migration algorithm (which yields the input for the inversion). Usually migration schemes account for geometrical spreading but not for transmission loss, which means the information in the data vectors $\mathbf{d}$ is distorted to some extent. In the next section we discuss how to compensate for this distortion.

Accounting for the effects of fine layering. Extensive studies on wave propagation through finely layered media have shown that transmission losses and internal multiple scattering result in an angle-dependent dispersion of the seismic waveform. Hence, ignoring these effects in migration yields dispersed images and erroneous AVA effects. Apart from these propagation-related distortions, the interference of the reflection responses of reflector packages ("composite reflectors") in finely layered media causes apparent AVA effects as well.

In order to account for the effects of fine layering in migration, a 3-D *generalized primary* representation of seismic reflection data has been developed (Figure 5). S^+ represents the source for downgoing waves at source point $\mathbf{x}_s$, W_g^+ describes generalized downward propagation into the subsurface (including transmission losses and internal multiple scattering), $\hat{R}$ is an operator that describes reflection at any point $\mathbf{x}$ in the subsurface, W_g^- describes generalized upward propagation to the surface, and P^- represents the upgoing wavefield at the receiver point $\mathbf{x}_R$. Note that this representation does not account for surface-related multiples. In the following, we shall assume that decomposition and surface-related multiple elimination have been carried out.

In essence, migration based on this representation ("generalized primary migration") is accomplished by applying the inverse versions of the propagators W_g^+ and W_g^- to the data P^-, thus resolving the reflectivity operator $\hat{R}$. For finely layered media, the inverse propagators cannot be approximated by the complex conjugate forward propagators.

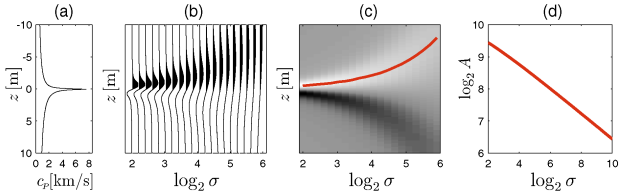

Figure 8. Multiscale analysis of a self-similar singularity. The slope in d ($\alpha = -0.4$) corresponds to the singularity exponent of the function in a.

Correction operators are required that compensate for the transmission losses. Using reciprocity, these transmission losses, and hence the correction operators, can be estimated from the reflection measurements at the surface. The inverse propagators that are thus constructed compensate for the propagation-related apparent AVA effects of fine layering. A modified imaging step compensates for the reflection-related apparent AVA effects (wavelet interference) of fine layering.

An example of an angle-dependent reflectivity section obtained by generalized primary migration of data modeled in a real well log is shown in Figure 6a, together with the well log of the *P*-wave velocity (Van Geloven et al., 1996 *SEG Expanded Abstracts*). The angle-dependent amplitude information in the data vector **d** at $z = 890$ m is in green in Figure 6b. It matches very well with the black curve, which represents the exact angle-dependent amplitude curve at the same depth. For comparison, the blue curve shows the angle-dependent reflectivity obtained by migration without the fine layering corrections. Clearly generalized primary migration

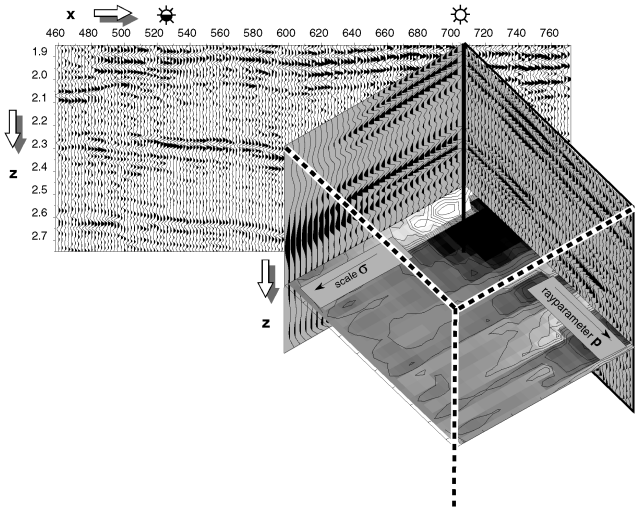

Figure 9. Integration of a structural image, an angle-dependent reflectivity section, and its multiscale representation (Van Wijngaarden and Verhelst). The p, σ-plane is used in multiscale AVA inversion.

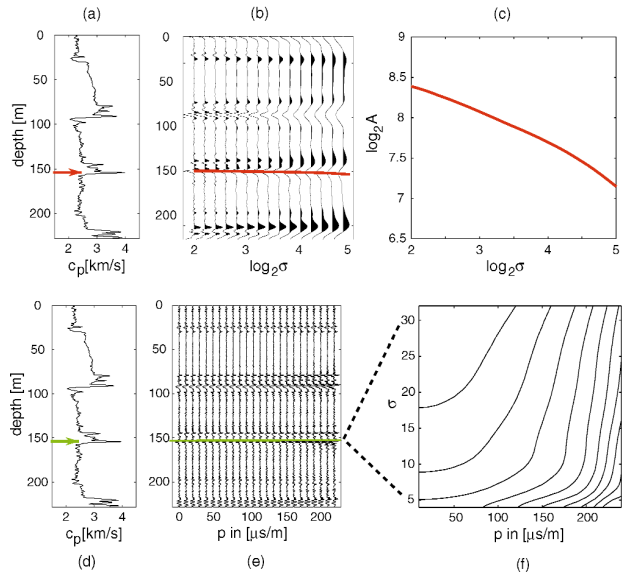

Figure 10. (a-c) Multiscale analysis of a singularity in a well log: $\alpha = -0.32$. (d-f) Multiangle, multiscale analysis of its seismic response: $\alpha = -0.34$.

yields improved angle-dependent reflectivity sections. We applied the AVA inversion method to a migration result without fine-layering corrections (not shown) and to the generalized primary migration result (Figure 6a). The estimated *P*-wave velocity contrasts ($\Delta c_p/\bar{c}_p$) are shown in Figures 7a-b by the blue and green curves, respectively. The black curves in both figures are appropriately band-filtered versions of $\Delta c_p/\bar{c}_p$, obtained directly from the well log. Note that the inversion result obtained after generalized primary migration (Figure 7b) matches the filtered velocity log quite accurately. A more detailed discussion of the effects of fine layering and examples with multimode data will appear in the November-December issue of GEOPHYSICS.

In summary, generalized primary migration not only accounts for geometrical spreading but also compensates for the dispersive transmission losses and wavelet interference related to fine layering. As a result, the apparent AVA effects are suppressed, so that the data vectors **d** are optimally suited as input for AVA inversion. Note that, for our AVA inversion, we assumed that the data vector **d** is related to the contrast parameter vector **λ** via linearized Zoeppritz equations, which implies that the medium parameters are assumed to behave as step functions of the depth coordinate z, at least in a finite interval around the reflector. From multiscale well-log analyses carried out by Herrmann (1997 doctoral dissertation, Delft University), it appears that outliers in well logs may behave quite differently from step functions. In the next section we discuss how to account for "composite reflectors" in AVA inversion.

Multiangle, multiscale inversion. In order to account for the complex behavior of outliers in well logs, we would like to generalize the parameterization of interfaces in such a way that their properties match those of real outliers and that the step-function interface can be seen as a special case. To this end we introduce the following singular function for the *P*-wave velocity:

$$c_p(z) = \begin{cases} c_1 |z|^{\alpha} \text{ for } z < 0 \\ c_2 |z|^{\alpha} \text{ for } z > 0 \end{cases} \qquad (1)$$

For convenience the singular point has been chosen at z

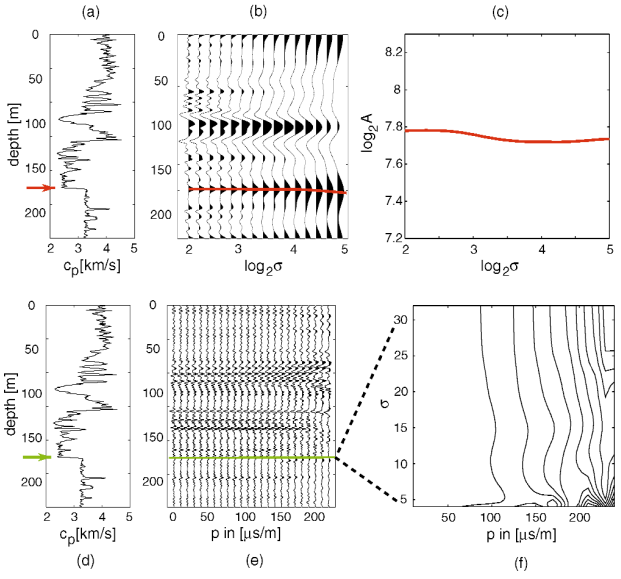

Figure 11. (a-c) Multiscale analysis of a step function in a well log: $\alpha = 0.0$. (d-f) Multiangle, multiscale analysis of its seismic response: $\alpha = 0.03$.

= 0. For $\alpha = 0$ this function reduces to a step function. For arbitrary α this function is self-similar, according to $c_p(\beta z) = \beta^{\alpha} c_p(z)$, for $\beta > 0$. For $\alpha = -0.4$, this function is shown in Figure 8a. We applied a multiscale analysis, following the method of Mallat and Hwang (IEEE *Transactions of Information Theory*, 1992) and Herrmann (1997). Figure 8b shows the continuous wavelet transform $\check{c}_p(\sigma,z)$ of this function, obtained by convolving $c_p(z)$ with scaled versions of an analyzing wavelet $(1/\sigma)\psi(z/\sigma)$, the derivative of a Gaussian. The different traces in Figure 8b correspond to different scales σ. Taking the modulus of the data in Figure 8b and connecting the local maxima from trace to trace yields the modulus maxima line (Figure 8c). Figure 8d shows the amplitudes measured along this line in a log-log plot. The slope of this amplitude-versus-scale (AVS) graph corresponds to the singularity exponent $\alpha = -0.4$ of the self-similar function in Figure 8a. For a step function, the slope of the AVS curve would be zero, meaning that a step function is scale-*in*dependent. The AVS behavior in Figure 8d is similar to that of several outliers in real well logs, as analyzed by Herrmann. This indicates that the parameterization of equation (1) is a useful generalization of the usual step-function interface. Note, however, that for real well logs the AVS curves reveal a "constant-slope" behavior only for a finite range of scales. Since seismic data are band limited anyway, it is sufficient that our parameterization is realistic in a finite scale range.

In order to resolve the multiscale reflector properties from seismic data rather than from the well log, a similar multiscale analysis as discussed above should be applied to the seismic data. Dessing (1997 doctoral dissertation, Delft University) applied the wavelet transform to unmigrated and migrated seismic data. Here we modify his procedure to multiangle, multiscale inversion. This is the subject of Goudswaard's Ph.D. research. Figure 9 shows the continuous wavelet transform of the angle-dependent reflectivity section of Figure 1. The z, σ-plane (for $p = 0$) was obtained in a similar way as that in Figure 8b. The same procedure was applied for all available p values, leading to a z, p, σ cube (dashed lines in Figure 9). The p, σ-plane (i.e., the horizontal cross-section in Figure 9) is a modulus maxima plane, built of modulus maxima lines (similar to those in Figure 8c) for all available p values; gray represents amplitudes in this modulus maxima plane. Note that this plane may be seen as a multiscale representation of the data vector **d** in Figure 1.

The aim of multiangle, multiscale inversion is to resolve the parameters of composite reflectors from the type of p, σ-planes illustrated in Figure 9. This requires a forward model that defines the multiangle, multiscale reflection behavior of composite reflectors. In the November-December issue of GEOPHYSICS, we show that, for a singularity described by equation (1), the contours of constant amplitude in the p, σ-plane are described by $p^{1-\alpha}\sigma^{\alpha}$ = constant. Hence, the singularity exponent a can be resolved by analyzing these contours. This is illustrated with examples in Figures 10 and 11. Figures 10a-c show a multiscale analysis of a real well log, analogous to Figure 8. The slope of the AVS curve in Figure 10c ($\alpha = -0.32$) characterizes the singularity at $z = 155$ m in the well log of Figure 10a. Figures 10d-f show a multiangle, multiscale analysis of the migrated seismic response, analogous to Figure 9 (only the angle-dependent reflectivity section and the p,σ-plane at $z = 155$m are shown). Using a contour-matching algorithm, it appears that the contours in Figure 10f are approximately described by $p^{1-\alpha}\sigma^{\alpha}$ = constant, with $\alpha = -0.34$. Note that this corresponds very well to the value obtained directly from the well log. Figure 11 shows a similar example, but this time the analyzed singularity at $z = 170$ m clearly resembles a step function. Note that the contours in Figure 11f show that for this situation there is hardly any scale dependency, as expected (the contours are approximately described by p = constant).

In summary, multiangle, multiscale inversion has the potential to resolve the parameters that characterize a composite reflector. What we have discussed in this section is the first step toward a general approach to multiangle, multiscale inversion. In the end, we would like to resolve the elastic and petrophysical parameters of composite reflectors and relate their multiscale parameters to the type of geologic facies. ℰ

Acknowledgments: We thank the sponsors of the DELPHI consortium project and its scientific director, Prof. A. J. Berkhout, in particular with regard to the research described in the section on multiangle inversion. Also the support of the Dutch Technology Foundation STW is highly appreciated.

Corresponding author: Kees Wapenaar, C.P.A.Wapenaar@CTG.TUDelft.nl